

# Parametric Discrete Morse Theory

A Master Semester Project

Written by Luca Massimo Nyckees

Supervised by Celia Hacker & Stefania Ebli



Laboratory for Topology and Neuroscience  
Directed by Prof. Kathryn Hess Bellwald  
Spring semester of 2021

## Contents

<b>1</b>	<b>Introduction</b>	<b>4</b>
<b>2</b>	<b>Smooth Morse Theory</b>	<b>6</b>
<b>3</b>	<b>Simplicial Complexes</b>	<b>9</b>
<b>4</b>	<b>CW-Complexes</b>	<b>11</b>
<b>5</b>	<b>Discrete Morse Theory</b>	<b>11</b>
<b>6</b>	<b>Parametric Morse Theory</b>	<b>18</b>
6.1	An Analogy with the Smooth Case . . . . .	23
<b>7</b>	<b>On Building Discrete Morse Functions</b>	<b>24</b>
7.1	Algorithm . . . . .	24
<b>8</b>	<b>An Application</b>	<b>28</b>
8.1	Morse features of finite node-function sequences . . . . .	28
8.2	Towards Robustness . . . . .	30
<b>9</b>	<b>Results</b>	<b>34</b>
9.1	The Tetrahedron . . . . .	34
9.2	The Triangle . . . . .	37
9.3	The Stochastic Block Model . . . . .	40
<b>10</b>	<b>What next?</b>	<b>43</b>
	<b>References</b>	<b>45</b>

### Abstract

Discrete Morse theory has recently found various interesting applications across different related domains of applied mathematics, such as homology computation and topological data analysis. It was developed as a discretized version of the classical smooth Morse theory, by Robin Forman (see [Forman]). Discrete Morse theory opened the gate to an approach called *parametric Morse theory* (see [B&D]). Parametric Morse theory introduces the notions of *birth* and *death* of critical cells along a sequence of discrete Morse functions  $\{f_t : K \rightarrow \mathbb{R}\}_{t=1}^n$  on a simplicial complex  $K$ . This approach produces life diagrams (or birth-death diagrams), which can be seen as enriched persistence diagrams for critical cells. We use the term «enriched» in the sense that not only do we get birth and death coordinates of critical cells, but also a further insight into their global behavior, e.g. when a critical cell *mutes* or *evolves* into another critical cell. We consider parametric Morse theory as a toolbox to analyse a sequence of vertex real-valued functions on a simplicial complex  $K$ . Moreover, we provide an implementation of the pipeline that can be found at the GitHub repository below (see Section 1).

### Acknowledgments

For their support throughout this whole learning experience, their advice and their ideas, I would like to thank Celia Hacker and Stefania Ebli, who supervised this project and guided me until the end. For the general advice and the help with the code, I am very thankful to Kevin Knudson, Harish Kannan, and Areejit Samal. And finally, for making all of this possible, my sincerest thanks go to Kathryn Hess Bellwald, the director of the *Laboratory for Topology and Neuroscience* at EPFL.

## 1 Introduction

Discrete Morse theory is a discrete version of smooth Morse theory developed by Robin Forman, as a tool to study the geometry and topology of discrete structures in algebraic topology. It has various applications in the domain of applied mathematics, from configuration spaces to computing homology groups. The aspect we are interested in is the application of discrete Morse theory to topological data analysis. In particular, we consider *parametric Morse theory*, a theoretical setting in which one can define the notions of *birth* and *death* of critical cells across a sequence of discrete Morse functions  $\{f_t : K \rightarrow \mathbb{R}\}_{t=1}^n$  defined on a simplicial complex  $K$ . This opens the way to interesting applications in the analysis of network dynamics. It was notably used to detect cavities in a human brain via voxelized data in [B&D].

Parametric Morse theory studies the time-related behavior of critical cells, which are thus the fundamental object of our study. To understand them well, we dedicate a part of this report to the presentation of smooth, discrete and parametric Morse theories. We give an explanation to relate the notions of life coordinates (birth and death) in the smooth and discrete cases.

For completeness, we recall the basic objects of algebraic topology that are dealt with in discrete Morse theory. We introduce simplicial complexes and CW-complexes in Section 3 and Section 4 respectively. Section 2 and Section 5 respectively deal with smooth and discrete Morse theories. We introduce smooth Morse theory in a less detailed way, as its only purpose here is to make an analogy with the concepts of birth and death in the discrete case.

In this project, we describe a method to analyse the topological features of a sequence of node labelings on a fixed graph  $G$ . More precisely, we consider a sequence of graph node labelings where each labeling in time is determined by a mapping that associates to each node a specific real-valued continuous function. The output of the pipeline are the birth and death diagrams of critical cells that appear along the sequence. Birth and death diagrams can be thought of as persistence diagrams for critical cells. We further investigate the robustness of the whole process by controlling the final impact of a possible perturbation of the initial node functions.

The general pipeline is implemented in Python, and the code is available at

the GitHub repository

<https://github.com/LucaNyckees/ParametricMorseTheory>.

The setting of parametric Morse theory is described in Section 6. Section 7 is dedicated to the description and implementation of **Algorithm 1** in [Saucan et al.2019]. This is an algorithm designed to extend a node function  $g : K^{(0)} \rightarrow \mathbb{R}$  on a simplicial complex  $K$  to a discrete Morse function  $f : K \rightarrow \mathbb{R}$ . Furthermore, it attains close to the theoretical minimal number of critical cells. In Section 8, we describe in detail the pipeline mentioned above. Results are presented in Section 9. In this section, we run the pipeline and investigate the robustness analysis. We consider in particular a stochastic block model defined via an approach of biological modeling of neural networks.

## 2 Smooth Morse Theory

In this section, rather than trying to provide a rigorous introduction to the basics of smooth Morse theory, we simply describe a motivating example. Of course, discrete Morse theory has its own applications, but it is always interesting to understand the links between the smooth case and the discrete case. This not only give an intuition on the matter, but also helps understand why we deal with certain objects in discrete Morse theory.

In the following, let  $M$  be a generic smooth manifold.

**Notation.** In this section, the notation  $A \cong B$  indicates the existence of a homeomorphism between the two topological spaces  $A$  and  $B$ .

**Definition 2.1** (Critical point). *Let  $f : M \rightarrow \mathbb{R}$  be a smooth map. A point  $x \in M$  is said to be critical for  $f$  provided that we have  $df_x = 0$ .*

At critical points of a map  $f : M \rightarrow \mathbb{R}$ , we are able to define the notion of *Hessian* as follows.

**Definition 2.2** (Hessian at critical points). *Let  $f : M \rightarrow \mathbb{R}$  be a map, and let  $x \in M$  be critical for  $f$ . We define the Hessian of  $f$  at  $x$ , denoted  $(df_x)^2$ , by setting*

$$(df_x)^2(X, Y) := X \cdot (\tilde{Y} \cdot f)(x)$$

*for all  $X, Y \in T_x M$ , where  $T_x M$  is the tangent space of  $M$  at  $x$  and  $\tilde{Y}$  is a local extension of  $Y$ .*

We say of a critical point  $x$  of a map  $f : M \rightarrow \mathbb{R}$  that is is non-degenerate if the Hessian of  $f$  at  $x$  is non-singular.

**Definition 2.3** (Morse function). *A smooth map  $f : M \rightarrow \mathbb{R}$  is a Morse function if all its critical points are non-degenerate.*

**Example 2.4** (Intuition with a 2-torus). *We choose any embedding of the 2-torus  $\mathbf{T}$  in the Euclidean space  $\mathbb{R}^3$ , and consider a height function on  $\mathbf{T}$ , that projects any point of  $M$  to the vertical axis, as shown in Figure 1. We denote the height function by  $p : \mathbf{T} \rightarrow \mathbb{R}$ .*

*The critical values are those for which the gradient of the height function vanishes and whose Hessian is non-singular. In this example, they are characterized by saddle points, local maxima and local minima. The non-degeneracy assumption for Morse functions ensures that we do not have*

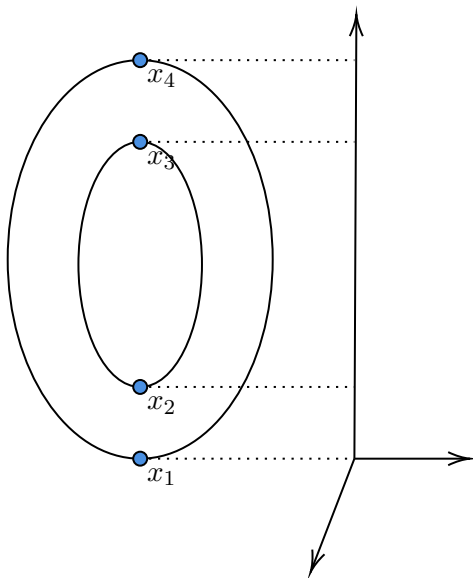


Figure 1: Critical points of a projection defined on the 2-torus.

*non-isolated critical points. For example, if we replaced the torus by a vertical cylinder, then the points on top of the cylinder have vanishing gradient, but their Hessian is singular.*

*The idea behind Morse functions is that they capture enough information about the manifold  $M$ . This means we avoid maps  $M \rightarrow \mathbb{R}$  for which critical points are situated at affine subvarieties of  $M$ , like plateaux. The important feature about critical points is that they encode the height levels at which the topology of the Morse function's level sets changes. More precisely, we consider a Morse function  $f : M \rightarrow \mathbb{R}$  and define subspaces of  $M$  of the form  $M_a := f^{-1}([-\infty, a])$ . If we progressively increase  $a \in \mathbb{R}$ , we find that the values at which we observe changes in the topology of the set  $M_a$  are precisely the heights of the critical points of  $f$ , i.e. the elements of the set  $\{f(x) | x \text{ is critical}\}$ .*

*For example, with notations of Figure 1, for all  $a, b \in [p(x_1), p(x_2)[$ , one has  $M_a \cong M_b$ . In this interval, the level sets are all circles. When increasing the height to a value of  $p(x_2)$ , the level set becomes a wedge of two circles, and going further gives the union of two disjoint circles. This provides us with a filtration of the underlying topological space  $\mathbf{T}$ , where each step indicates*



a topological change :

$$\emptyset \subset M_{p(x_1)} \subset M_{p(x_2)} \subset M_{p(x_3)} \subset M_{p(x_4)} = \mathbf{T}.$$

Given a Morse function  $f : M \rightarrow \mathbb{R}$ , we introduce the notions of *stable* and *unstable* manifolds of a critical point of  $f$ . These concepts play a crucial role in making a link between the smooth case and the discrete case, when considering the notions of birth and death of critical cells (see Section 6).

First, we recall some notions of differential geometry. For a Morse function  $f : M \rightarrow \mathbb{R}$ , and a critical point  $x \in M$ , one can approximate the  $f$ -values of points  $y$  in an appropriate neighborhood of  $x$  can be approximated by the expression

$$f(y) \sim f(x) + \frac{(d^2f)_x(y-x, y-x)}{2}.$$

This follows from Taylor's theorem, recalling that the gradient of  $f$  vanishes at  $x$  since it is a critical point. A *Morse chart* of  $x$  is a neighborhood of  $x$  such that this approximation is actually an equality. Such charts always exist, by the so-called «Morse lemma».

**Definition 2.5** (Pseudo-gradient). *Let  $f : M \rightarrow \mathbb{R}$  be a function. A pseudo-gradient for  $f$  is a vector field  $X$  satisfying*

- (a)  $(df_x)(f) \leq 0$  for all  $x \in M$ ,
- (b)  $(df_x)(f) = 0$  if and only if  $x \in M$  is critical,
- (c) On any Morse chart around a critical point  $x$ , the vector fields  $X$  and  $-\text{grad}(f)$  coincide.

**Definition 2.6** ((Un)stable Manifolds). *Let  $f : M \rightarrow \mathbb{R}$  be a Morse function, and let  $x \in M$  be a critical point of  $f$ . Consider a pseudo gradient field  $X$  for  $f$ , and let  $\phi^t$  denote the vector flows of  $X$ . The stable and unstable manifolds of  $x$  are defined, respectively, as*

$$W^s(x) = \{y \in M \mid \lim_{t \rightarrow \infty} \phi^t(y) = x\}, \text{ and}$$

$$W^u(x) = \{y \in M \mid \lim_{t \rightarrow -\infty} \phi^t(y) = x\}.$$

**Example 2.7** ((Un)stable manifolds). *We look at a manifold  $N$  embedded into  $\mathbb{R}^3$ , with associated height function  $p : N \rightarrow \mathbb{R}$ , as shown in Figure 2. The height function  $p$  is Morse, and has four critical points, denoted*

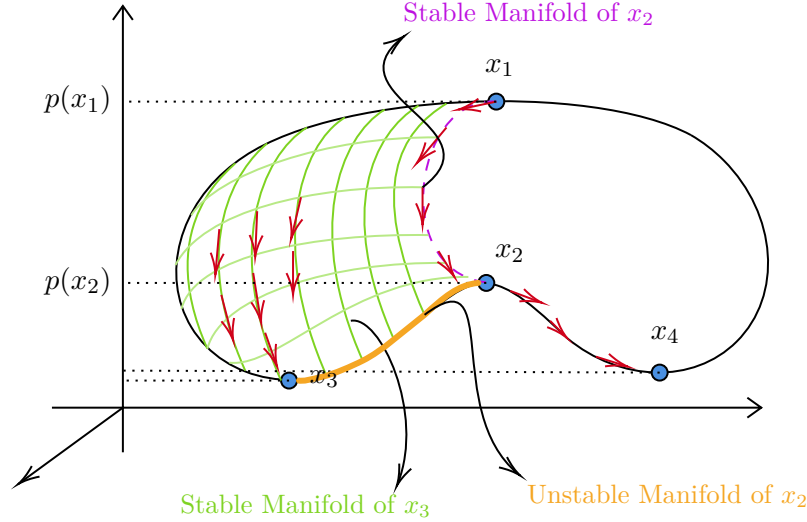


Figure 2: Stable and unstable manifolds of critical points with respect to a height function defined of a manifold  $N$  embedded in  $\mathbb{R}^3$ . The red arrows represent a vector flow  $\phi : N \times \mathbb{R} \rightarrow \mathbb{R}$  of the vector field  $\text{grad}(p)$ .

$x_1, \dots, x_4$ . We consider a vector flow  $\phi^t$ , indicated by red arrows in the figure. Roughly speaking, the stable manifold of a critical point  $x_i$  consists in the set of points of  $N$  that are the starts of some paths in the vector flow  $\phi^t$  ending up at  $x_i$ . Conversely, the unstable manifold of a critical point  $x_i$  is the set of points that are the endpoints of some paths in the vector flow starting at  $x_i$ .

For example, we have  $W^u(x_1) = N$ , as any point of the manifold is the endpoint of a path starting at  $x_1$ . Moreover, the stable manifold of  $x_2$  is a circle passing through the points  $x_1$  and  $x_2$ . Indeed, it consists of the only points of  $N$  that are the start of a path ending in  $x_2$ . More examples are illustrated in Figure 2.

### 3 Simplicial Complexes

A simplicial complex is a set of simplices (generalized triangles, e.g. tetrahedrons) that are glued together in a way that respects a specific hierarchy. More precisely, we have the following definitions. First, we recall the definition of *geometric simplex* to get a «Euclidean» intuition on simplices. That

said, we shall only consider *abstract simplices* later on.

**Definition 3.1** (Geometric Simplex). *Let  $k \in \mathbf{N}$ . A  $k$ -dimensional simplex (or  $k$ -simplex)  $\alpha$  is the convex hull built on a set of affinely independent points  $V = \{v_0, \dots, v_{k+1}\} \subset \mathbb{R}^k$ . Symbolically, one has*

$$\alpha = \left\{ \sum_{i=0}^k a_i v_i \mid (a_i)_{i=0}^k \in \mathcal{C}_k \right\}$$

where we define the set  $\mathcal{C}_k = \{(a_i)_{i=0}^k \mid \sum_{i=0}^k a_i = 1\} \cap \mathbb{R}_+^{k+1}$ .

It follows that simplices are, apart from vertices and edges, higher dimensional triangles (e.g. tetrahedrons). For example, a 2-simplex is a triangle, a 3-simplex is a tetrahedron and a 4-simplex is a 4-cell (homeomorphic to the disk  $D^4$ ). *Regular  $k$ -simplices* are just  $k$ -simplices where, with notations as in the definition above, the points  $v_1, \dots, v_k$  are the standard unitary vectors of  $\mathbb{R}^k$  and  $v_0 = \mathbf{0}$ . Simplices are most often studied up to homotopy, *i.e.* continuous deformation. Thus, one can always consider the case of regular simplices and imagine nice regular triangles and tetrahedrons. We define the *face* of a  $k$ -simplex to be a convex hull built on a subset (that is not the entire simplex) of the points that constitute the  $k$ -simplex. Faces are simplices themselves. For two simplices  $\alpha$  and  $\beta$ , we denote by  $\alpha < \beta$  (or equivalently  $\beta > \alpha$ ) the fact that  $\alpha$  is a face of  $\beta$ .

**Definition 3.2** (Abstract Simplex). *An abstract simplex  $\sigma$  is a finite set of vertices of the form  $\{v_i\}_{i=0}^n$ , which we denote by  $\sigma = [v_0, \dots, v_n]$ . An abstract  $n$ -simplex is an abstract simplex built on  $n$  vertices.*

**Definition 3.3** (Abstract Simplicial Complex). *An abstract simplicial complex  $X$  is a set of abstract simplices such that both conditions (1) and (2) expressed below are satisfied.*

$$(1) \quad \beta < \alpha \in X \implies \beta \in X$$

$$(2) \quad \alpha, \beta \in X \text{ and } \alpha \cap \beta \neq \emptyset \implies \alpha \cap \beta < \alpha \text{ and } \alpha \cap \beta < \beta$$

When considering an abstract simplicial complex, we shall simply use the term *simplicial complex*. Simplicial complexes can be obtained from graphs by completing some cliques, in the sense that we add higher-dimensional relations between edges, as we do when we consider hypergraphs, for example. Simplicial complexes are the structure we choose for running the experiments of this project, since they are the most natural object on which to define discrete Morse theory.

## 4 CW-Complexes

Although we do not use CW-complexes in our computations, this class of objects plays an important role in understanding the basics of discrete Morse theory, especially in the formulation of «minimal decomposition» results (e.g. Theorem 5.9). In particular, they lead to very elegant analogies with the case of smooth Morse theory, and thus meaningful interpretations.

CW-complexes are topological spaces that are built inductively, by attaching cells progressively to some original space. We have the following definitions.

**Definition 4.1** (Cellular attachment). *Let  $X$  be a topological space and let  $n \in \mathbb{N}$ . Let  $e^n$  be an  $n$ -cell (i.e. homeomorphic to the  $n$ -disk) and consider a continuous map  $f : S^{n-1} \rightarrow X$ . The glued space  $X \cup_f e^n$  is the topological space that makes the diagram below commute.*

$$\begin{array}{ccc} S^{n-1} & \xrightarrow{f} & X \\ i \downarrow & & \downarrow \\ D^n & \longrightarrow & X \cup_f e^n \end{array}$$

*The glued space  $X \cup_f e^n$  is said to be obtained by attaching an  $n$ -cell to  $X$  via the gluing application  $f : S^{n-1} \rightarrow X$ . The map  $i : S^{n-1} \rightarrow D^n$  is the natural embedding application of the boundary of the disk  $D^n$  into itself.*

**Definition 4.2** (CW-complex). *A CW-complex is a space  $X$  that can be obtained by induction on a chain of the form  $X_0 \subset X_1 \subset \dots \subset X_d = X$ , where the space  $X_i$  is obtained from attaching a cell to the space  $X_{i-1}$ .*

## 5 Discrete Morse Theory

In this section, we introduce the notion of *discrete Morse theory*, as defined by Robin Forman (see [Forman]), and have a look at some of its related fundamental results.

**Notation.** For the entirety of sections 5 and 6, we consider a generic simplicial complex  $K$ . We shall also denote its underlying set of simplices as  $K$ , for practical purposes. For a simplex  $\alpha \in K$ , we denote by  $\mathcal{B}_\alpha^F$  and  $\mathcal{B}_\alpha^C$  the sets of its codimension-1 faces and cofaces, respectively. Finally, we shall use the symbol  $\simeq$  to denote a homotopy equivalence of two spaces.

**Definition 5.1.** Let  $f : K \rightarrow \mathbb{R}$  be a real-valued function. If conditions (1) and (2) below are satisfied, we say  $f$  is a discrete Morse function on  $X$ .

$$(1) \sum_{\beta \in \mathcal{B}_\alpha^F} \mathbb{1}_{\{f(\beta) \geq f(\alpha)\}} \leq 1, \forall \alpha \in K$$

$$(2) \sum_{\beta \in \mathcal{B}_\alpha^C} \mathbb{1}_{\{f(\beta) \leq f(\alpha)\}} \leq 1, \forall \alpha \in K$$

The idea behind such a function is that, with at most one break of the rule, it assigns numbers to simplices in an increasing way, when considering the ordering given by the binary relation  $\alpha \prec \beta \iff \dim(\alpha) < \dim(\beta)$ .

**Definition 5.2.** If the sums in Definition 5.1 are both zero for the same given simplex  $\alpha \in K$ , then we say that  $\alpha \in K$  is a critical simplex. We will denote by  $\text{Cr}_i^f(X)$  the set of  $i$ -dimensional critical cells of  $X$  with respect to the discrete Morse function  $f : K \rightarrow \mathbb{R}$ .

We now put those concepts in practise, by considering the case of the sphere. It is worth the time to make a link with smooth Morse theory. For a smooth manifold  $M$  with homeomorphic simplicial complex  $Y$ , we have the following correspondence, provided that the simplicial decomposition attains the minimum number of critical cells (this is explained later on): critical 0-cells, critical 1-cells and maximum-dimensional critical cells of  $Y$  correspond to local minima, saddle points and local maxima, respectively.

**Example 5.3** (Discrete Morse function on the sphere  $S^2$ ). Let us consider the simplicial complex  $X$  given by a triangulation of the sphere  $S^2$  in Figure 3, where edges and vertices are identified as shown by the coloring. We build a discrete Morse function on  $X$  as described by the values on the vertices and edges. This way, we obtain exactly one critical vertex and one critical 2-cell, namely the vertex with value 9 and the 2-cell with value 21.

We see this agrees with the note above : those critical cells indicate the existence of exactly one local maximum and one local minimum of  $S^2$  when considering the smooth Morse theory approach.

We come to the main result of discrete Morse theory. It resonates with the observation that the sphere  $S^2$  admits a CW-complex decomposition made of one 0-cell and one 2-cell (we build the sphere by contracting the boundary of a disk  $D^2$  to a point, i.e. we attach a 2-cell to a 0-cell).

**Theorem 5.4.** Let  $f : K \rightarrow \mathbb{R}$  be a discrete Morse function on a simplicial complex  $X = (V, K)$ . Then  $X$  admits a homotopy equivalent CW-complex decomposition consisting of exactly  $|\text{Cr}_i^f(X)|$   $i$ -cells.

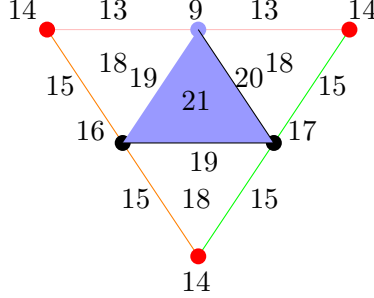


Figure 3: A discrete Morse function on  $S^2$ . The two critical cells (a vertex and a triangle) are highlighted in violet (taking Morse values 9 and 21).

Before giving a proof of Theorem 5.4, we make a few observations.

**Definition 5.5.** Let  $\alpha < \beta$  be simplices in  $X$ . If  $\beta$  is the only coface of  $\alpha$ , then we say  $\alpha$  is a free face of  $\beta$ .

**Remark 5.6.** Whenever we have an inclusion of simplicial complexes  $X_a \subset X_b$  such that  $X_b \setminus X_a = \{\alpha, \beta\}$ , where  $\alpha$  is a free face of  $\beta$ , we can find a deformation retraction from  $X_b$  to  $X_a$ . This process of deformation retraction by canceling exactly two simplices is called a simplicial collapse. For example, one can collapse a triangle to a point in three steps of simplicial collapsing. We say that the triangle is collapsible. ♠

**Notation.** Given our generic simplicial complex  $K$ , we define, for any real value  $x \in \mathbb{R}$ , a subcomplex of  $K$  by setting  $K(x) := \cup_{\alpha < \beta} \cup_{\beta \in f^{-1}(x)} \beta$ .

**Proposition 5.7.** Let  $x < y$  be two values in  $\mathbb{R}$ . If  $K(y) \setminus K(x)$  contains no critical cell, then we can deformation retract  $K(y)$  to  $K(x)$ .

*Proof.* If no critical cells are contained in  $K(y) \setminus K(x)$ , it means we only have pairs of regular cells. By the definition of a discrete Morse function, given a pair of regular cells  $\alpha < \beta$ ,  $\alpha$  is necessarily a free face of  $\beta$ . Hence, we can obtain a series of simplicial collapses, which proves the claim. ■

**Proposition 5.8.** Let  $x < y$  be two values in  $\mathbb{R}$ . If the set  $K(y) \setminus K(x)$  contains exactly one critical cell  $\alpha^{(d)}$  for some  $d \in \mathbb{N}$ , then we can find a gluing map  $g : S^{d-1} \rightarrow D^d$  so that we have a glued space  $K(x) \cup_g D^d \simeq K(y)$ .

*Proof.* One obtains  $K(y)$  by adding  $\alpha^{(d)}$  to  $K(x)$  in a way that coincides with attaching a  $d$ -cell to  $K(x)$ . Indeed,  $\alpha^{(d)}$  is a  $d$ -cell and it is glued to

$K(x)$  by being patched to its boundary. This follows from the fact that  $\alpha$  is critical : its boundary already belongs to  $K(x)$ . For example, if  $d = 2$  we would patch a 2-cell to an empty triangle, obtaining a cell  $e^2$ . Hence, what we really do each time is adding a critical cell of dimension  $d$  to a subcomplex which is covering (or patching) a  $d - 1$ -dimensional hole of  $K(x)$ . ■

*Proof of Theorem 5.4.* Let us consider a filtration

$$K(x_0) \subset K(x_1) \subset \cdots \subset K(x_m) = K,$$

where  $\{x_0, \dots, x_m\}$  is precise enough so that each complement set of the form  $K(x_i) \setminus K(x_{i-1})$ ,  $i \in \{1, \dots, m\}$ , contains either no critical cell or exactly one critical cell. Then it follows from the two propositions above that  $K$  is obtained, up to homotopy equivalence, by consecutively attaching the critical cells of the Morse function  $f$ . Indeed, if  $\{x_{j_0}, \dots, x_{j_k}\} \subseteq \{x_0, \dots, x_m\}$  represents the steps of the filtration in which we add the critical cells, then we know that  $K$  has a CW-complex decomposition given by the filtration

$$K(x_{j_0}) \subset K(x_{j_1}) \subset \cdots \subset K(x_{j_k}).$$

Hence the result. ■

Now, one may wonder why this result is important. What it tells us is that finding a *good* Morse function on a simplicial complex  $X$ , *i.e.* with a minimal number of critical cells, ensures that there exists a *good* CW-complex decomposition of  $X$ , *i.e.* with a minimal number of cells in each dimension. This minimality refers to the proof of the result below, that mathematically answers the question *how well can we do?*



**Theorem 5.9** (Morse Inequalities). *Let  $m_d$  denote the number of critical  $d$ -simplices for some discrete Morse function  $f : K \rightarrow \mathbb{R}$  on  $K$ , let  $b_d = \dim(H_d(K))$ , and let  $c_d$  denote the number of  $d$ -cells appearing in some CW-complex decomposition of  $X$ . One obtains*

$$(1) \ b_d \leq m_d \ \forall d \in \{0, \dots, \dim(K)\},$$

$$(2) \ b_d \leq c_d \ \forall d \in \{0, \dots, \dim(K)\}.$$

*Proof.* By using Theorem 5.4, it is easy to see that proving condition (2) is sufficient. We state and prove a family of inequalities, from which condition (2) is quickly deduced. In fact, we show that for any  $d \in \{0, \dots, \dim(K) + 1\}$ , one has  $\sum_{i=0}^{d-i} c_i \geq \sum_{i=0}^{d-i} b_i$ . This follows from the calculation provided below, where  $\delta_i : C_i(X) \rightarrow C_{i-1}(X)$  are the boundary maps used to define the homology theory of  $CW$ -complexes ( $C_i(X)$  is the  $\mathbb{Z}$ -module generated by the  $i$ -cells appearing in the  $CW$ -complex decomposition of  $X$ ). One has

$$\begin{aligned} \sum_{i=0}^d (-1)^{d-i} b_i &= \sum_{i=0}^d (-1)^{d-i} \dim(H_i(X)) \\ &= \sum_{i=0}^d (-1)^{d-i} [\dim(\ker(\delta_i)) - \dim(\operatorname{im}(\delta_{i+1}))] \\ &= \sum_{i=0}^d (-1)^{d-i} \dim(\ker(\delta_i)) + \sum_{i=0}^d (-1)^{d-i+1} \dim(\operatorname{im}(\delta_{i+1})) \\ &= \sum_{i=0}^d (-1)^{d-i} \dim(\ker(\delta_i)) + \sum_{i=1}^{d+1} (-1)^{d-i} \dim(\operatorname{im}(\delta_i)) \\ &= \sum_{i=0}^d (-1)^{d-i} \dim(\ker(\delta_i)) + \sum_{i=0}^d (-1)^{d-i} \dim(\operatorname{im}(\delta_i)) \\ &\quad - (-1)^d \dim(\operatorname{im}(\delta_0)) - \dim(\operatorname{im}(\delta_{d+1})) \\ &= \sum_{i=0}^d (-1)^{d-i} \dim(C_i(X)) - \dim(\operatorname{im}(\delta_{d+1})) \\ &= \sum_{i=0}^d (-1)^{d-i} c_i - \dim(\operatorname{im}(\delta_{d+1})) \\ &\leq \sum_{i=0}^d (-1)^{d-i} c_i, \end{aligned}$$

where we use that  $\dim(\operatorname{im}(\delta_0)) = 0$ . ■

Manually constructing a discrete Morse function can easily become complicated when considering non-trivial simplicial complexes. For this reason, a recurring question in discrete Morse theory is the way we should build algorithmically discrete Morse functions. There are algorithms designed to



execute this task in a rather efficient way (e.g. in [King et al.2005] or [Saucan et al.2019]). Before presenting one of these algorithm, we will now present a nice tool allowing to better understand the geometry of discrete Morse functions, namely the notion of *gradient vector field*. We use the notation  $\gamma^{(p)}$  to indicate the fact that a simplex  $\gamma$  is a  $p$ -simplex.

**Definition 5.10** (Discrete vector field). *We define a discrete vector field  $V$  on  $K$  to be a set of pairs  $\{\alpha^{(p)} < \beta^{(p+1)}\} \in K \times K$  such that  $|A_\gamma| \leq 1$  for each  $\gamma \in K$ , where we define the set  $A_\gamma := \{(\alpha, \beta) \in V \mid \gamma \in \{\alpha, \beta\}\}$ .*

**Definition 5.11** ( $V$ -path). *Let  $V$  be a discrete vector field on  $K$ . A  $V$ -path is a finite sequence of simplices of the form  $\{\alpha_1^{(p)}, \beta_1^{(p+1)}, \dots, \alpha_n^{(p)}, \beta_n^{(p+1)}, \alpha_{n+1}^{(p)}\}$  such that  $(\alpha_i, \beta_i) \in V$  satisfy the relations  $\alpha_i < \beta_i > \alpha_{i+1}$  and  $\alpha_i \neq \alpha_{i+1}$  for all  $i \in \{1, \dots, n\}$ . Such a  $V$ -path is a  $V$ -cycle provided that  $\alpha_1 = \alpha_{n+1}$ .*

We consider again a discrete Morse function  $f : K \rightarrow \mathbb{R}$ . One observes that non-critical (or *regular*) simplices come in pairs: suppose  $\alpha \in K$  is a codimension-1 face of  $\beta \in K$  with  $f(\alpha) \geq f(\beta)$ . Then, by symmetry,  $\beta \in K$  is a codimension-1 coface of  $\alpha \in K$  with  $f(\beta) \leq f(\alpha)$  and, by definition of discrete Morse function, this inversion they share is their only inversion (*i.e.* they belong to no other such pair). Now, in this case, we adopt the convention of drawing an arrow from  $\alpha$  to  $\beta$ , so as to get an ordered pair  $(\alpha, \beta) \in K \times K$ , which we call a *regular pair*. A *gradient vector field* of  $f$  is a discrete vector field that is built with respect to  $f$ , meaning that its pairs are regular pairs in the sense described above.

**Definition 5.12** (Gradient vector field). *Let  $f : K \rightarrow \mathbb{R}$  be a discrete Morse function on  $K$ . A gradient vector field of  $f$  is a discrete vector field  $V = \{(\alpha, \beta)\}$  where each pair  $(\alpha, \beta)$  is a regular pair.*

A connected finite sequence of arrows (*i.e.* regular pairs) is a *gradient path*.

**Definition 5.13** (Gradient path). *Let  $V$  be a discrete vector field on  $K$ , and  $f : K \rightarrow \mathbb{R}$  a discrete Morse function on  $K$ . A  $V$ -path is a gradient path of  $f$  if  $V$  is a gradient vector field of  $f$ .*

Now, we observe that gradient paths of a discrete Morse function  $f : K \rightarrow \mathbb{R}$  are in particular sequences along which  $f$  takes decreasing values. With notations as in the definition above, one has the inequalities below.

$$f(\alpha_1) \geq f(\beta_1) > f(\alpha_2) \geq f(\beta_2) > f(\alpha_3) \geq \dots$$

Indeed, let us fix  $i \in \{1, \dots, n\}$ . Then  $f(\alpha_i) \geq f(\beta_i)$  follows from the fact that  $(\alpha_i, \beta_i)$  is a regular pair. *Ab absurdo*, suppose that  $f(\beta_i) \leq f(\alpha_{i+1})$ .

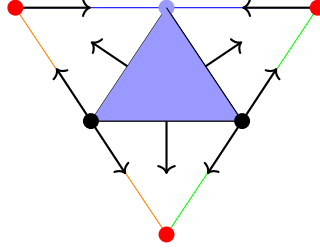


Figure 4: Discrete vector field on a triangulation of the sphere  $S^2$ . In purple are the two critical cells. The identifications of the triangulation between the various simplices are indicated with same coloring.

Then, since  $\alpha_{i+1}$  is a face of  $\beta_i$ , we have that  $(\alpha_{i+1}, \beta_i)$  is a regular pair. But regular pairs are pairwise disjoint and thus  $\alpha_i = \alpha_{i+1}$ , a contradiction. What is elegant about this is the fact that the converse is true as well.

**Proposition 5.14.** *Let  $V$  be a gradient vector field of some discrete Morse function  $f$ . Then a finite sequence  $\{\alpha_1^{(p)}, \beta_1^{(p+1)}, \dots, \alpha_n^{(p)}, \beta_n^{(p+1)}, \alpha_{n+1}^{(p)}\}$  is a gradient path iff we have*

- (1)  $\alpha_i < \beta_i$  and  $\beta_i > \alpha_{i+1}$  for all  $i \in \{1, \dots, n\}$
- (2)  $f(\alpha_1) \geq f(\beta_1) > f(\alpha_2) \geq f(\beta_2) > f(\alpha_3) \geq \dots$

As a consequence, gradient paths do not form cycles. It turns out that the converse statement is also true, i.e. discrete vector fields with no cycles admit some potential. We can say a discrete vector field  $V$  is derived from a potential  $f$  if  $V$  is the gradient vector field of the discrete Morse function  $f$ . More precisely, we formulate the result below.

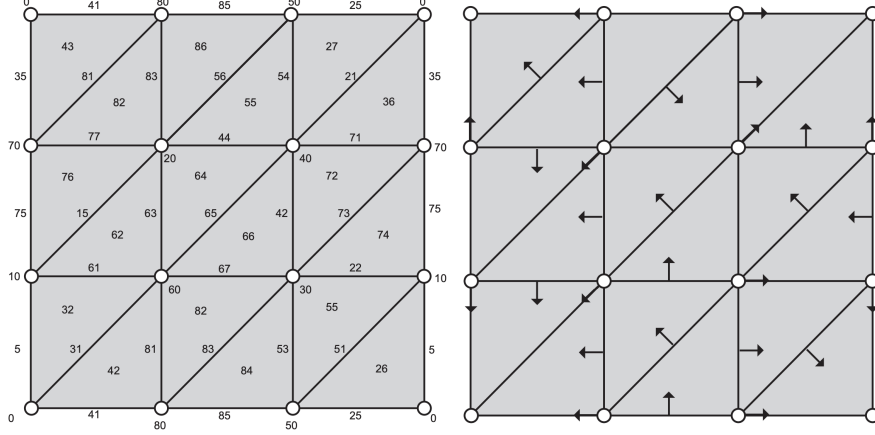
**Theorem 5.15.** *For any discrete vector field  $V$  with no cycles, there exists a discrete Morse function  $f : K \rightarrow \mathbb{R}$  for which  $V$  is a gradient path.*

*Proof.* See [Forman]. ■

**Example 5.16** (Discrete vector field on the sphere  $S^2$ ). *We go back to the sphere  $S^2$ , triangulated as a tetrahedron. One can build a discrete vector field as the set of arrows shown in Figure 4. This is the gradient vector field of the Morse function exhibited in Example 5.3.*

**Remark 5.17** (General flow behavior). *Generally speaking, an interesting phenomenon can be seen : following the arrows along a maximal path leads to a critical cell. One can play around with the gradient vector field build on*

the 2-dimensional torus below (example borrowed from [King et al.2005]). But we also note that not all critical cells can be accessed from following a path. For example, the cell with value 21, critical for our Morse function built on  $S^2$ , is not the endpoint of any path.



## 6 Parametric Morse Theory

In this section, we lay the foundations of *parametric Morse theory*, a theory developed by H. King, N. Mramor and K. Knudson in the paper [B&D]. In this paper they consider a method aiming to understand the evolution of critical cells in a parameter-varying network (e.g. a time parameter). More precisely, they look at a given sequence  $\{f : X \rightarrow \mathbb{Z}\}_{f \in \mathcal{F}}$  of discrete Morse functions each defined on the same fixed simplicial complex  $X$ , and try to track the behavior (*i.e.* the apparition and the persistence) of critical cells. Once again, this has been done in the case of smooth Morse theory, from which one can build an intuition; moreover, the links between the two theories, especially in regard of parametric Morse theory, is a domain full of open questions. We refer to Section 7 of [B&D] for insights into related future work.

**Remark 6.1.** Here, we consider the case where the simplicial complex decomposition  $X$  of the space we consider does not change through time. The general case, in which the simplicial complex can change through time, is treated in Section 4 of [B&D]. This is done by introducing the notions of cellulation refining and discrete vector field refining. ♠

**Definition 6.2.** A finite Morse parametrization of  $X$  is a sequence of the form  $\{(f_i, V_i)\}_{i=1}^n$  where  $\{f_i : X \rightarrow \mathbb{R}\}_{i=1}^n$  is a family of discrete Morse functions on  $X$  and for  $i \in \{1, \dots, n\}$ ,  $V_i$  is the gradient vector field of  $f_i$ .

For any  $k$ , we now define the notions of *strong* and *forward connections* between two  $k$ -cells of  $X$ , each critical for some Morse functions  $f_i$  and  $f_j$ , respectively. For the remainder of the section, we consider a finite Morse parametrization  $\{(f_i, V_i)\}_{i=1}^n$  of  $X$ . We denote by  $X^l$  the set of  $l$ -cells of  $X$ .

**Definition 6.3.** Let  $\alpha_i$  and  $\alpha_j$  be  $k$ -cells of  $X$ , critical for  $f_i$  and  $f_j$  respectively, for some  $i \neq j \in \{1, \dots, n\}$ . We say there is a *forward connection* from  $\alpha_i$  to  $\alpha_j$ , provided the existence of a  $k$ -cell  $\gamma$  with a  $V_i$ -path  $\{\alpha_i, \dots, \gamma\} \subseteq X^{k-1} \cup X^k$  and a  $V_j$ -path  $\{\gamma, \dots, \alpha_j\} \subseteq X^k \cup X^{k+1}$ . If there is a forward connection from  $\alpha_i$  to  $\alpha_j$  and vice-versa, we say that there is a *strong connection* between the two cells. Two critical cells sharing a strong connection are said to be *strongly connected*.

**Definition 6.4.** Let  $\alpha \in K$  be a cell that is critical for  $V_i$ . We say  $\alpha$  is *born* (resp. *dies*) at index  $i$  provided that no strong connection exists between  $\alpha$  and any cell that is critical for  $V_{i-1}$  (resp.  $V_{i+1}$ ). If there is cell  $\beta \in K$  that is critical for  $V_{i+1}$ , such that the only strong connection of  $\alpha$  and  $\beta$  is between themselves, then we say  $\alpha$  *moves* (or *mutes*) to  $\beta$ .

Now, just as one can plot the bifurcation diagram of a family of smooth Morse functions  $\{f_i : \mathbb{R} \rightarrow \mathbb{R}\}_{i \in I}$ , where  $I$  is the unit interval (*i.e.* plotting the evolution of the critical points in the plane  $\mathbb{R} \times I$ ), one can consider what we call the *birth-death diagram* of a finite Morse parametrization of  $X$ . Thus, instead of continuous curves in the plane, we look at point sequences in the plane that trace the behavior of critical cells as the time parameter changes. Birth-death diagrams encode the connectivity of critical cells across the «time-line».

**Example 6.5** (Birth-Death diagram). As an example, we consider a cellulation of the circle  $S^1$ , as it is rather simple space on which to generate various discrete vector fields. We take the same vector fields as in Figure 4 of [B&D] (figures 5 and 6 below are borrowed from this reference). In Figure 7, the evolution of the time parameter is illustrated clockwise.

**Definition 6.6** (Parametric diagram). We define the *parametric diagram* of a finite Morse parametrization  $\{(f_i, V_i)\}_{i=1}^n$  to be the subset of the space  $(\mathbb{R}_+)^2$  formed by the diagonal  $D = \{(x, x)\}_{x \in \mathbb{R}_+}$  and the set of birth-death coordinates of all critical cells in the parametrization.

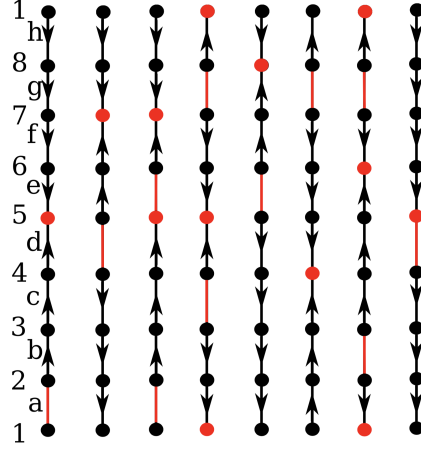


Figure 5: A Morse parametrization on  $S^1$  for Example 6.5. The critical cells are indicated with red coloring. This figure is borrowed from [B&D].

**Remark 6.7.** *In a way, parametric diagrams are analogous to persistence diagrams. The difference is that we do not consider the usual topological features but rather critical cells.* ♠

**Remark 6.8.** *A parametric diagram encodes less information than the corresponding birth-death diagram. Indeed, in a birth-death diagram, one can easily retrieve the life coordinates of critical cells, and can further observe the behavior of critical cells through connectivity curves.* ♠

**Remark 6.9.** *The passage from the setting of gradient vector fields to the drawing of birth-death diagrams relies, of course, on finding all possible forward and strong connections between critical cells. To this end, an algorithm was developed in [B&D], to which we refer for more complex examples. This algorithm is implemented in the code we provide on GitHub.* ♠

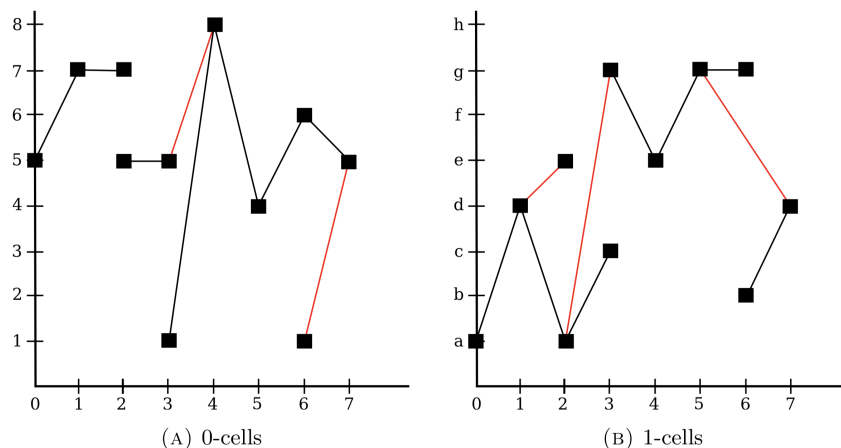


Figure 6: The birth-death diagram for Example 6.5. The strong connections are indicated with black coloring. This figure is borrowed from [B&D].

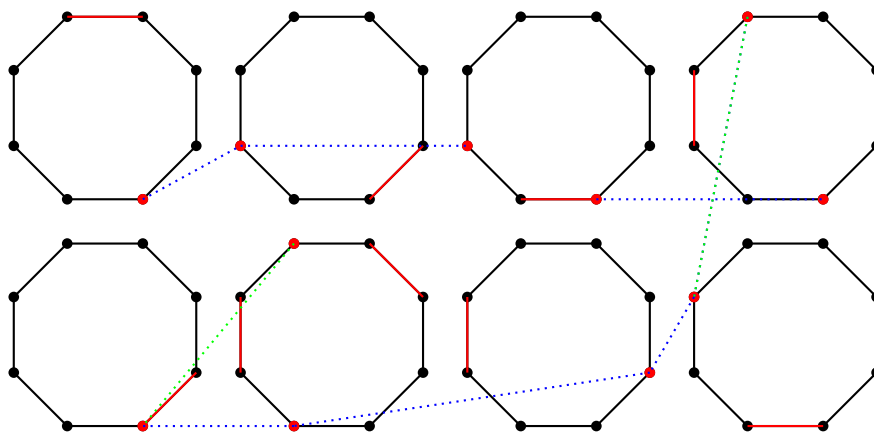


Figure 7: Continuation of Example 6.5 - this is a compact visualization for the case of 0-cells : blue edges represent strong connections, green edges represent simple forward connections. To read in the clockwise direction. Critical cells are emphasized in red color. One can imagine that we bent the natural timeline into a  $U$ -shaped curve.

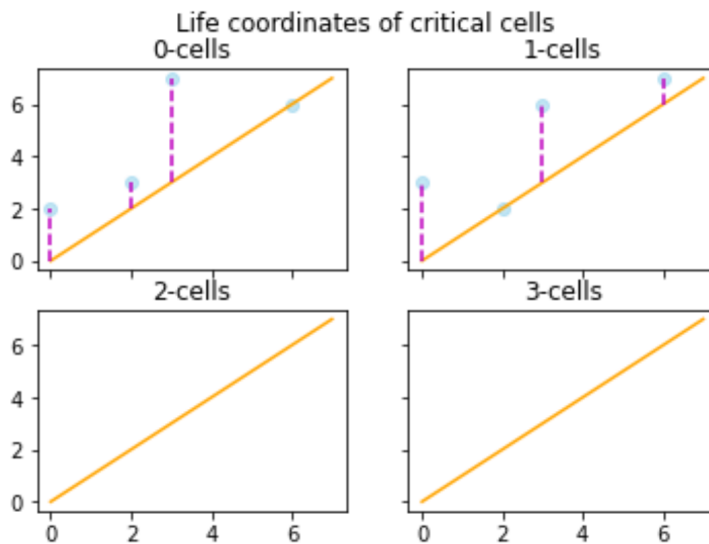
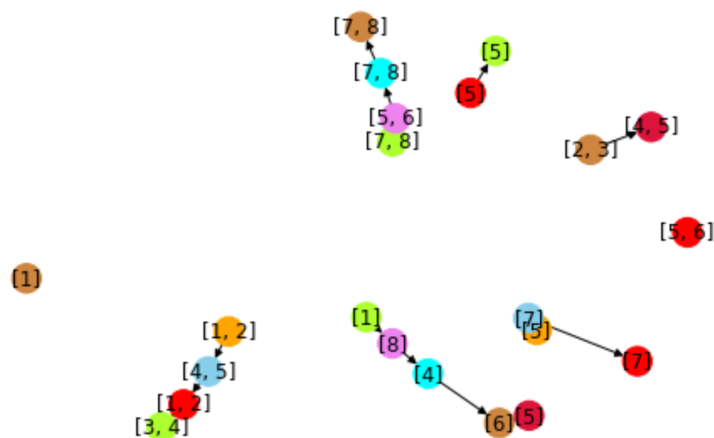


Figure 8: The parametric diagram for Example 6.5.


 Figure 9: A visualization of connectivity information for Example 6.5. Each critical cell is colored according to its associated time-slice. There is a time slice where cell  $[2, 3]$  mutates into cell  $[4, 5]$ .

### 6.1 An Analogy with the Smooth Case

Let  $M$  be a smooth manifold. The notions of birth and death in smooth Morse theory are notions that naturally appear by considering a family of smooth Morse functions  $\{f_t : M \rightarrow \mathbb{R}\}_{t \in \mathbb{R}}$  such that the function  $f : M \times \mathbb{R} \rightarrow \mathbb{R}$ :

$$f : \begin{cases} M \times \mathbb{R} \rightarrow \mathbb{R} \\ (x, t) \mapsto f_t(x) \end{cases}$$

is smooth. We suggest an analogy as described in Figure 6.1.

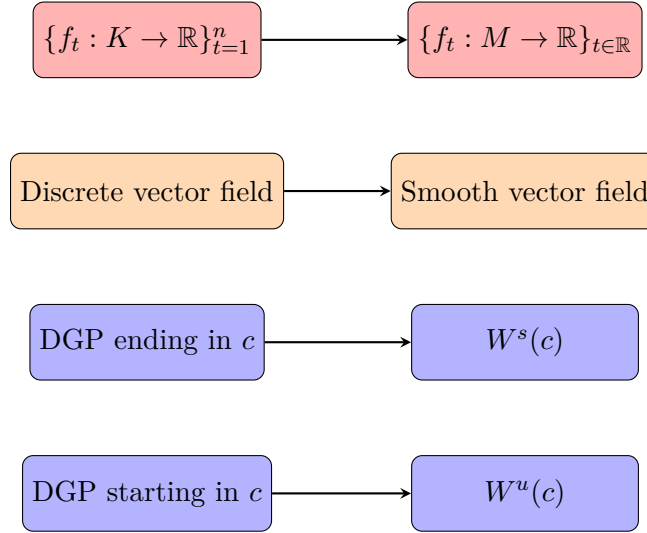


Figure 10: An analogy for the notions of birth and death of critical cells in the smooth case versus the discrete case. We use «DGP» for «discrete gradient path».

**Idea.** We observe the following. We define the notions of birth and death of critical cells in a finite Morse parametrization with the gradient path existence condition «There is a  $k$ -cell  $\gamma$  with a  $V_i$ -path  $\{\alpha_i, \dots, \gamma\} \subseteq X^{k-1} \cup X^k$  and a  $V_j$ -path  $\{\gamma, \dots, \alpha_j\} \subseteq X^k \cup X^{k+1}$ .» This translates to the smooth Morse theory setting as a condition of the form «There is a point  $x \in M$  such that  $x \in W^u(c_i) \cup W^s(c_j)$ .», where  $c_i \in M$  (resp.  $c_j \in M$ ) is the critical point corresponding to critical cell  $\alpha_i$  (resp.  $\alpha_j$ ).



The smooth setting in which the study of time-related behavior of critical cells is the *Cerf theory*, to which we refer to for deeper insights into the subtleties of the smooth case.

## 7 On Building Discrete Morse Functions

As said before, a great deal in discrete Morse theory is how to build or generate discrete Morse functions. In most real-life applications, we are given a set of point data, and thus we usually start working with simplicial complexes with vertex values. An important step, to apply the theory we have seen, is thus to extend a vertex-valued function to a discrete Morse function on the whole complex. Various algorithms based on the notions of discrete vector field and *Hasse diagram* exist, and we refer in particular to [King et al.2005] for a detailed example of algorithm (here we shall work with an implementation described in [Saucan et al.2019]). In the first paper mentioned above, the authors propose an implementation allowing one to extend any injective function defined on a 0-skeleton  $h : K_0 \rightarrow \mathbb{R}$  to a discrete Morse function  $\tilde{h} : K \rightarrow \mathbb{R}$  in a way that preserves the global behavior of  $h$ . Moreover, the algorithm involves a way of deleting pairs of critical cells, to a certain degree. More precisely, one can choose a *persistence level*  $p \in \mathbb{R} \cup \{\infty\}$  so that pairs of critical cells that are connected by exactly one gradient path (with respect to a temporary discrete Morse function based on  $h$ ) and whose difference of  $h$ -values is lower than  $p$ , are canceled. This process aims not only at canceling a maximum of critical cells (with  $p = \infty$ ) so as to simplify homology computations, for example, but also at deleting topological features that are noise-related (with  $p \in \mathbb{R}$ ) since those usually do not persist through time for too long.

### 7.1 Algorithm

Although the method in [King et al.2005] is designed with a very attractive way of perceiving critical cells, we choose to run our experiments with another, more recent algorithm that is more practical and easier to implement. More precisely, we follow **Algorithm 1** of [Saucan et al.2019], whose pseudo-code is reported below. Moreover, we provide an implementation of the code written in Python, making use of the *Gudhi* library. For a given simplicial complex, the output function achieves close to the theoretical minimum of critical cells. In the code hereunder, the variable `Flag[]`

encodes the numbers

$$n_\alpha := \sum_{\beta \in \mathcal{B}_\alpha^F} \mathbb{1}_{\{f(\beta) \geq f(\alpha)\}}$$

for each  $\alpha \in K$ , where we look at a simplicial complex  $K$ . Moreover, the input  $g$  denotes a function  $K^{(0)} \rightarrow \mathbb{R}$  defined on the vertices of the complex.

---

**Algorithm 1** Extending vertex labels to a discrete Morse function

---

```

1: procedure EXTENDTOMORSE( $K, g$ )
2:    $d \leftarrow \dim(K)$ 
3:   for  $p = 0, \dots, d$  do
4:     for  $\alpha^{(p)} \in K$  do
5:        $n_\alpha \leftarrow 0$ 
6:     for  $\alpha^{(0)} \in K$  do
7:        $f(\alpha) \leftarrow g(\alpha)$ 
8:     for  $p = 1, \dots, d$  do
9:       for  $\alpha^{(p)} \in K$  do
10:        Let Faces be a list of all  $(p-1)$ -dimensional faces of  $\alpha$ 
11:        Sort Faces by decreasing order of  $f$ -values
12:         $\gamma_0 \leftarrow \mathbf{Faces}[0]$ 
13:         $\gamma_1 \leftarrow \mathbf{Faces}[1]$ 
14:        if  $\mathbf{Flag}[\gamma_0] = 0$  and  $f(\gamma_0) > f(\gamma_1)$  then
15:           $f(\alpha) = (f(\gamma_0) + f(\gamma_1))/2$ 
16:           $\mathbf{Flag}[\gamma_0] \leftarrow 1$ 
17:        else
18:           $\epsilon \leftarrow \text{UniformRandom}(0, 0.5)$ 
19:           $f(\alpha) \leftarrow f(\gamma_0) + \epsilon$ 
20:   return  $f$ 

```

---

In the code, the function `getskel(K,p)` returns the set of  $p$ -cells of  $K$ . We choose to encode the label function  $f$  and the `Flag` variable as dictionaries `dict`, for practical implementation purposes. For example, if we have  $f([1,2,3]) = 2.1$  for some triangle  $[1,2,3] \in K$ , then the label dictionary `f` will contain an entry of the form `"[1,2,3]":2.1`.

---

```
// Extending vertex labels to a discrete Morse function
import gudhi as gd

def build_morse_function(K,d,g):
    """
    K : simplicial complex (gudhi.SimplexTree)
    d : dimension of K
    g : labels on nodes given by a dictionary
    """
    Flag = {}
    f = {}

    for p in range(d):
        for simplex in list(K.get_skeleton(p)):
            Flag[str(simplex[0])]=0

    for simplex in list(K.get_skeleton(0)):
        f[str(simplex[0])] = g[str(simplex[0])]

    for p in range(1,d+1):

        for simplex in getskel(K,p):
            Faces = [face[0] for face in
                    list(K.get_boundaries(simplex[0]))]
            Faces = [str(face) for face in Faces]
            Faces = sorted(Faces, key=lambda x: f[x], reverse=True)
            gamma_0 = Faces[0]
            gamma_1 = Faces[1]

            if (Flag[Faces[0]]==0 and f[gamma_0]>f[gamma_1]):
                f[str(simplex[0])]=(f[gamma_0]+f[gamma_1]) / 2
                Flag[gamma_0]=1

            else:
                epsilon = np.random.uniform(low=0.0, high=0.5)
                f[str(simplex[0])] = f[gamma_0] + epsilon

    return [f, Flag]
```

---

Simplex	function $f_1$	function $f_2$	Flag	IsCritical
[0]	3.1	3.1	1	False
[1]	2.1	2.1	1	False
[2]	1.1	1.1	0	True
[3]	3.2	3.2	1	False
[4]	3.3	3.3	1	False
[5]	3.4	3.4	1	False
[6]	4.1	4.1	1	False
[7]	0.1	0.1	0	True
[8]	4.3	4.3	1	False
[0,1]	2.60	2.60	0	False
[1,2]	1.60	1.60	0	False
[2,3]	2.15	2.15	0	False
[3,4]	3.25	3.45	0	False
[4,2]	3.45	2.2	1	False
[2,5]	2.25	2.25	0	False
[5,7]	3.48	3.52	0	True
[1,7]	2.35	2.37	0	True
[7,0]	3.15	3.57	1	False
[7,6]	2.10	2.10	0	False
[7,8]	2.20	2.20	0	False
[0,1,7]	2.875	3.086	0	False
[2,3,4]	3.350	2.825	0	False

Figure 11: Extending a vertex label to a discrete Morse function

**Example.** We reproduce the experiment of [Saucan et al.2019] (*cf.* Figure 1 of the paper), and compare the results. We note that we obtain the same final **Flag** values, as well as the same critical cells. However, note that we add a uniformly distributed random noise term in line 18 of the pseudo-code. Hence, the method contains a stochastic step and our output function thus slightly changes. We denote by  $f_1$  and  $f_2$  the discrete Morse functions reported in the experiment of [Saucan et al.2019] and with our code, respectively. The table in Figure 7.1 contains all the information on the input  $(K, g)$ ; indeed,  $K$  is formed of all simplices reported in the first column, and  $g$  is equal to the restriction of the functions  $f_1$  and  $f_2$  to the vertices.

## 8 An Application

### 8.1 Morse features of finite node-function sequences

In this subsection, we report the precise process we go through to analyse the discrete Morse features associated to a sequence of graphs with vertex values obtained from an initial input graph  $G$ .

**Clique completion.** We form a simplicial complex  $K$  obtained from the input graph  $G$  by clique completion.

**Assigning vertex values.** We form a sequence of pairs  $\{(K, g_t)\}_{t=1}^n$  where each  $g_t : K \rightarrow \mathbb{R}$  is a node labeling function, defined based on a parameter-dependent sampling process. More precisely, we choose an initial mapping

$$\mathbf{h} : \begin{cases} G \rightarrow \mathcal{C}^0(\mathbb{R}) \\ i \rightarrow h_i \end{cases},$$

where  $\mathcal{C}^0(\mathbb{R})$  denotes the space of continuous functions  $\mathbb{R} \rightarrow \mathbb{R}$ . Then, we choose a set of parameters  $(x_0, \delta, n) \in \mathbb{R} \times \mathbb{R} \times \mathbb{N}$  and define, for a given time slice  $t \in \{1, \dots, n\}$ , the function

$$g_t : \begin{cases} G \rightarrow \mathbb{R} \\ i \rightarrow g_t(i) := h_i(x_0 + t\delta) \end{cases}.$$

We illustrate this process in Figure 12.

**Generating Morse functions.** Now, we can obtain a family of discrete Morse functions  $\{(K, f_t)\}_{t \in [T]}$  by extending each  $g_t : K^{(0)} \rightarrow \mathbb{R}$  to a map  $f_t : K \rightarrow \mathbb{R}$  via the algorithm described in the previous section. Finally, we are able to run the full parametric Morse theory analysis on  $\{(K, f_t)\}_{t \in [T]}$ , *i.e.* we report, at each time slice  $t \in [T]$ , the current critical cells and the gradient vector field of  $f_t$ . Moreover, we can plot the corresponding parametric diagrams.

**Plotting parametric diagrams.** Finally, we are able to plot the parametric diagrams of the time-series  $\{(K, f_t)\}_{t \in [T]}$ . Those can be thought of, in some sense, as persistence diagrams for *all* critical cells of the complex  $K$

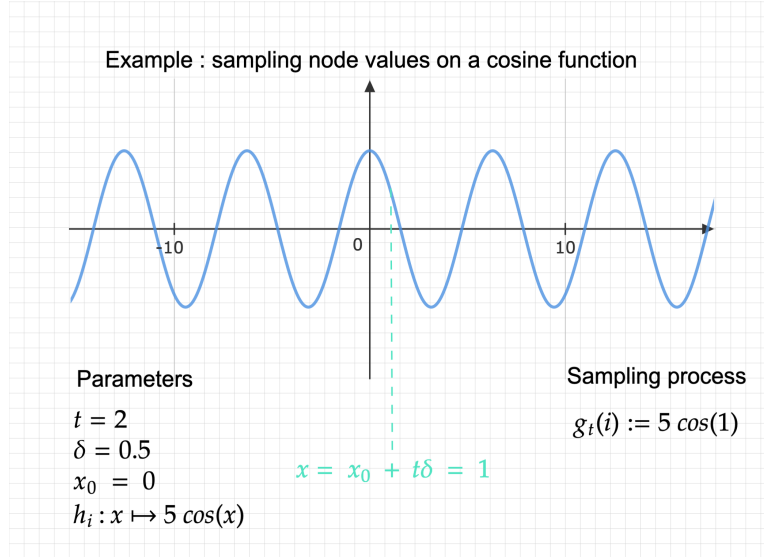


Figure 12: Sampling process illustrated for a node  $i$  and associated node function  $h_i : x \mapsto 5 \cos(x)$ , with parameters  $(x_0, \delta) = (0, 0.5)$  and time  $t = 2$ .

(i.e. with respect to all discrete Morse functions  $(f_t)_t$ ).

**Pipeline illustration.** Figure 8.1 illustrates the process followed by the pipeline, starting from a graph  $G$  together with node functions as input and obtaining parametric diagrams as output, through the steps described above.

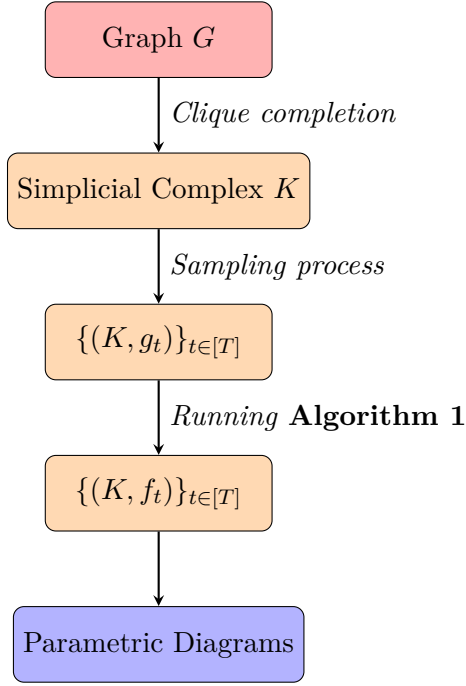


Figure 13: Main Pipeline. This diagram illustrates the process of obtaining parametric diagrams starting from an input graph  $G$ .

## 8.2 Towards Robustness

When following such a method, one can naturally think of the pipeline as a mapping

$$F : \mathcal{G} \rightarrow 2^{\mathbb{R} \times \mathbb{R}},$$

where  $\mathcal{G}$  is the set of all pairs of the form  $(G, \mathbf{h})$  where  $G$  is a graph and  $\mathbf{h} : G \rightarrow \mathcal{C}^0(\mathbb{R})$  is a mapping as described earlier. The mapping  $F$  sends the pair  $(G, \mathbf{h})$  to its associated parametric diagram. Following this way of thinking, one may wonder about the robustness of the method, or analogously about the *stability* of  $F$ . More precisely, given a perturbation in the early steps of the method, we look at how much the final output is affected. There are many ways of perturbing the method in the early steps. For example, one could try to answer this question by running the same experiment on a graph  $G$  two times, where the stochastic map  $\{(K, g_t)\}_{t \in [T]} \rightarrow \{(K, f_t)\}_{t \in [T]}$  is implemented with a significant amount of noise. This means we get two time-series  $\{(K, f_t)\}_{t \in [T]}$  and  $\{(K, \hat{f}_t)\}_{t \in [T]}$ . Instead, we choose another way

of considering perturbations, which we describe below.

**Perturbing the vertex values.** Let us consider the node functions setting described in Section 8.1, *i.e.* we have, for an input graph  $G$ , a mapping

$$\mathbf{h} : \begin{cases} G \rightarrow \mathcal{C}^0(\mathbb{R}) \\ i \rightarrow h_i \end{cases}.$$

and we choose a set of parameters  $(x_0, \delta, n) \in \mathbb{R} \times \mathbb{R} \times \mathbb{N}$  so as to define, for a fixed time slice  $t \in \{1, \dots, n\}$ , the function

$$g_t : \begin{cases} G \rightarrow \mathbb{R} \\ i \rightarrow g_t(i) := h_i(x_0 + t\delta) \end{cases}.$$

Now, we choose a *perturbation term*  $\varepsilon > 0$ , and define, for a fixed time slice  $t \in \{1, \dots, n\}$ , the *perturbed* node labeling function  $\tilde{g}_t$  by setting

$$\tilde{g}_t : \begin{cases} G \rightarrow \mathbb{R} \\ i \rightarrow \tilde{g}_t(i) := h_i(x_0 + t\delta + \varepsilon) \end{cases}.$$

For the stability analysis, we choose to define a distance between the two sequences of node labeling functions  $\mathbf{g} := \{g_t\}_{t=1}^n$  and  $\tilde{\mathbf{g}} := \{\tilde{g}_t\}_{t=1}^n$  by setting

$$d(\mathbf{g}, \tilde{\mathbf{g}}) := \frac{1}{n} \sum_{t=1}^n \|g_t - \tilde{g}_t\|_\infty,$$

where we set  $\|g_t - \tilde{g}_t\|_\infty := \max_{i \in G} |g_t(i) - \tilde{g}_t(i)|$ .

Let  $K > 0$  be fixed and suppose that, for each  $i \in G$ , the associated continuous function  $h_i \in \mathcal{C}^0(\mathbb{R})$  is  $L$ -Lipschitz. Then it follows that, for a perturbing term  $\varepsilon$ , and sequences  $\mathbf{g}$  and  $\tilde{\mathbf{g}}$  as above, one has

$$d(\mathbf{g}, \tilde{\mathbf{g}}) = \frac{1}{n} \sum_{t=1}^n \|g_t - \tilde{g}_t\|_\infty \tag{1}$$

$$= \frac{1}{n} \sum_{t=1}^n \max_{i \in G} |g_t(i) - \tilde{g}_t(i)| \tag{2}$$

$$= \frac{1}{n} \sum_{t=1}^n \max_{i \in G} |h_i(x_0 + t\delta) - h_i(x_0 + t\delta + \varepsilon)| \tag{3}$$

$$\leq \frac{1}{n} \sum_{t=1}^n L\varepsilon \tag{4}$$

$$= L\varepsilon, \tag{5}$$



and we are thus able to control the term  $d(\mathbf{g}, \tilde{\mathbf{g}})$ . For clarity purposes, we shall also denote the perturbed sequence  $\tilde{\mathbf{g}}$  by  $\mathbf{g}_\varepsilon$ , given that the associated perturbation term is  $\varepsilon$ .

**Evaluating the final impact.** The effect of perturbing vertex values on the final output is then evaluated in terms of distances between the resulting parametric diagrams. More precisely, we compute the Bottleneck and some  $p$ -Wasserstein distances (defined below) between parametric diagrams obtained with and without perturbation.

**Definition 8.1** (Bottleneck distance.). *For two diagrams  $D, \tilde{D} \in \mathbb{N} \times \mathbb{N}$ , we define their Bottleneck distance as*

$$d_B(D, \tilde{D}) = \inf_{h: D \rightarrow \tilde{D}} \sup_{x \in D} \|x - h(x)\|_\infty,$$

where the infimum is taken over all bijections  $h : D \rightarrow \tilde{D}$ . Note that a bijection is allowed here to send a point  $(x, y) \in D$  to the diagonal of the  $\tilde{D}$ .

**Definition 8.2** ( $p$ -Wasserstein distance.). *For two diagrams  $D, \tilde{D} \in \mathbb{R} \times \mathbb{R}$  of same cardinality, we define their  $p$ -Wasserstein distance as*

$$d_p(D, \tilde{D}) = \left\{ \inf_{h: D \rightarrow \tilde{D}} \sup_{x \in D} \|x - h(x)\|_\infty^p \right\}^{\frac{1}{p}}$$

where the infimum is taken over all bijections  $h : D \rightarrow \tilde{D}$ . Note that a bijection is allowed here to send a point  $(x, y) \in D$  to the diagonal of the  $\tilde{D}$ .

**Remark 8.3.** *Note that the Wasserstein distances provide a way to generalize the Bottleneck distance. Indeed, the Bottleneck distance is equivalent to the 1-Wasserstein distance, i.e.  $d_1(\cdot, \cdot) = d_B(\cdot, \cdot)$ .* ♠

We may consider a distance between two discrete Morse parametrizations as a kind of mean quadratic error summed over all time slices. However, in the results section, we only consider a perturbation on the vertex values and not directly on the function  $f : K \rightarrow \mathbb{R}$ . The danger with the second method is that we may obtain non-Morse functions by perturbing a discrete Morse function.

**Definition 8.4** (Parametric distance.). *We define a distance  $d$  between two time-series  $\{(K, f_t)\}_{t \in [T]}$  and  $\{(K, \tilde{f}_t)\}_{t \in [T]}$  as above by setting*

$$d\left(\{(K, f_t)\}_{t \in [T]}, \{(K, \tilde{f}_t)\}_{t \in [T]}\right) = \frac{1}{|G|} \frac{1}{T} \sum_{i \in G} \sum_{t \in T} (f_t(i) - \tilde{f}_t(i))^2.$$

The test of stability is illustrated in Figure 8.2 below. The set  $\mathcal{D} = (D_k)_k$  (resp.  $\tilde{\mathcal{D}} = (\tilde{D}_k)_k$ ) contains parametric diagrams obtained from the time-series  $\{(K, f_t)\}_{t \in [T]}$  (resp.  $\{(K, \tilde{f}_t)\}_{t \in [T]}$ ), where  $D_k$  (resp.  $\tilde{D}_k$ ) consists of  $k$ -dimensional cells exclusively. Thus, we compute the distances between parametric diagrams of  $k$ -critical cells, for some  $k \in \{0, \dots, \dim(K)\}$ .

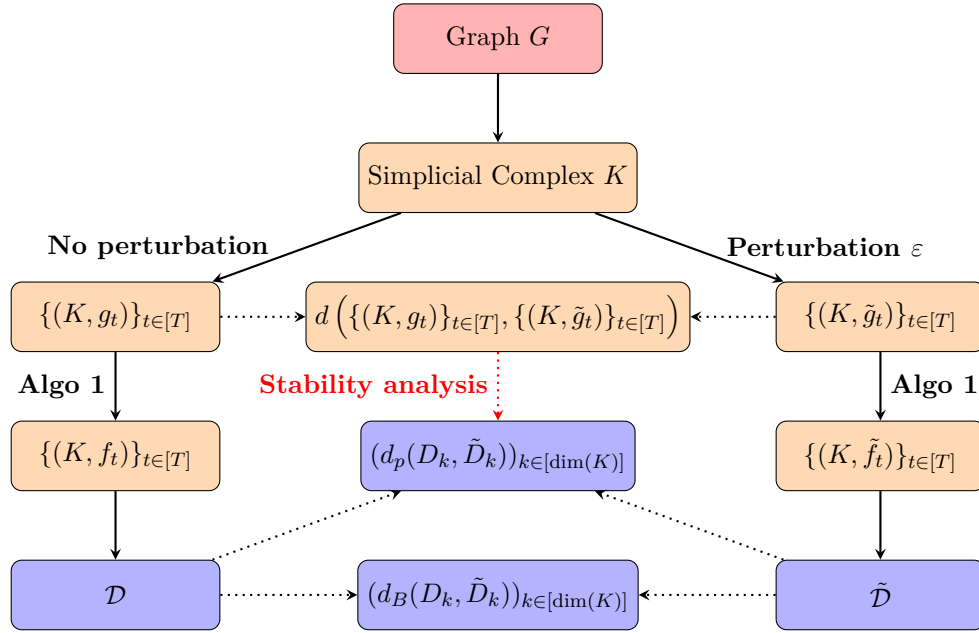


Figure 14: Testing stability process. This diagram illustrates the concept of the stability analysis : it consists of comparing the output of the pipeline when running it with and without a perturbation term.

**Remark 8.5.** Let  $D_k^\varepsilon$  denote the diagram  $\tilde{D}_k$  obtained by running the pipeline with perturbation term  $\varepsilon$ . For the continuity analysis to make sense, we have to translate the birth and death coordinates of a perturbed diagram by the perturbation term used. More precisely, if we run the pipeline with perturbation term  $\varepsilon$ , and obtain to sets of diagrams  $(D_k)_{k=1}^n$  and  $(D_k^\varepsilon)_{k=1}^n$ , then the births and deaths of a diagram  $D_k^\varepsilon$  will live in time-slices  $t = 1 + \varepsilon, \dots, n + \varepsilon$ . ♠

**Complete Analysis.** Our analysis further consists in computing and plotting a discrete curve

$$(\varepsilon, d(\mathbf{g}, \mathbf{g}_\varepsilon))_{\varepsilon \in E},$$

for some finite set  $E \subset \mathbb{R}^+$ , to observe how the node labeling functions react to perturbations. We compute and plot the curves

$$(\varepsilon, d_B(D_k, D_k^\varepsilon))_{\varepsilon \in E}$$

for  $k = 1, \dots, p$  where  $p$  is the maximum dimension of critical cells.

## 9 Results

In this section, we report the results of the continuity analysis described in Section 8.2. We run the tests on two graphs. We consider the example of the circle, and the sphere  $S^2$  triangulated as a tetrahedron.

### 9.1 The Tetrahedron

In this subsection, we consider our simplicial complex  $K$  to be a tetrahedron. We set  $G = K^{(0)}$ , and choose an associated constant mapping

$$\mathbf{h} : \begin{cases} G \rightarrow \mathcal{C}^0(\mathbb{R}) \\ i \rightarrow h \end{cases},$$

where  $h(x) = \cos(2x)$  for all  $x \in \mathbb{R}$ . First, we run the pipeline with no perturbation term. Hence we consider a single time sequence. More precisely, we choose the initial parameters so that we define

$$g_t : \begin{cases} G \rightarrow \mathbb{R} \\ i \rightarrow g_t(i) := h(5t) \end{cases},$$

where  $t \in \{0, \dots, 7\}$ . We have a sequence of 8 node labeling functions  $g_t : G \rightarrow \mathbb{R}$ . We run the experiment two times, and compare the two resulting birth-death diagrams shown in Figure 15 and Figure 16.

**Interpretation.** We observe that with a fixed noise term of  $\varepsilon = 0.05$  in the stochastic step of the extension algorithm (**Algorithm 1**), the outputs clearly differ. Now, we observe a common behavior between the two sets of diagrams. More precisely, we have a very high number of 0-cells appearing along the sequence, all of them having same birth-death coordinates. All

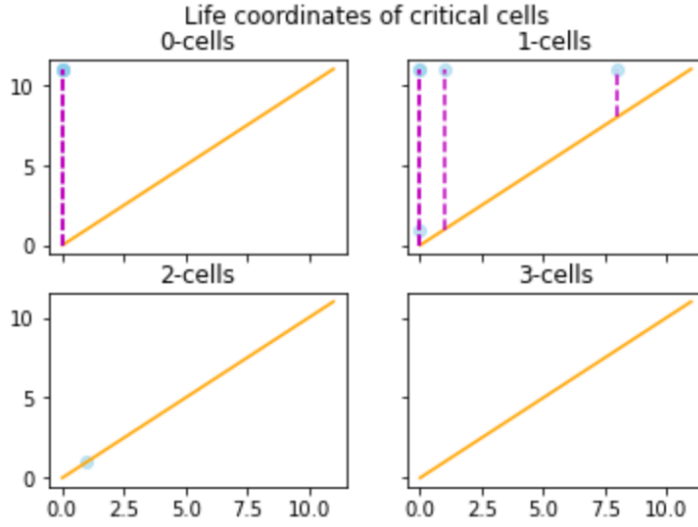


Figure 15: Parametric diagrams obtained with a tetrahedron as input and cosine waves on each vertex. Each parametric diagram corresponds to a specific dimension of critical cells, as indicated.

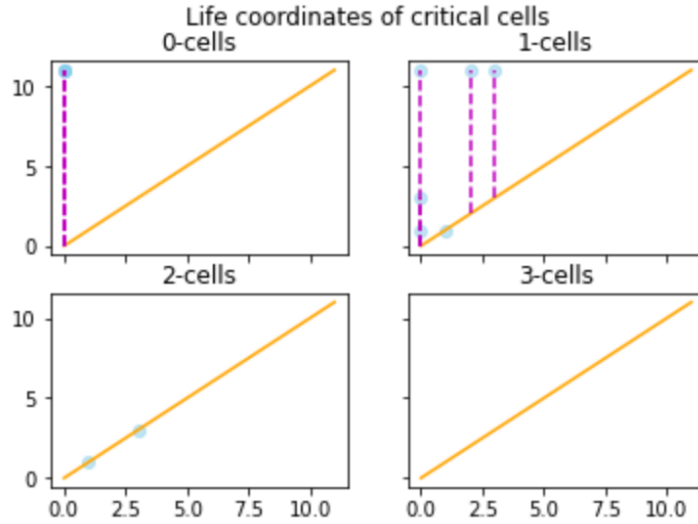


Figure 16: Parametric diagram obtained with a tetrahedron as input and cosine waves on each vertex. Each parametric diagram corresponds to a specific dimension of critical cells, as indicated.

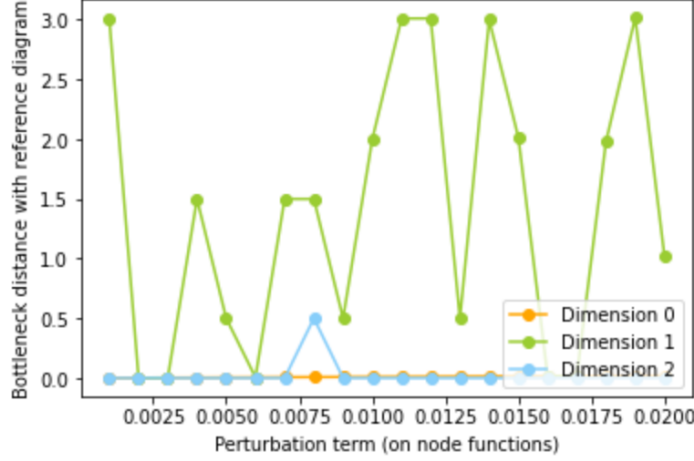


Figure 17: This figure represents the plotting of the curves  $(\varepsilon, d_B(D_k, D_k^\varepsilon))_{\varepsilon \in E}$  for the tetrahedron with cosine waves on each vertex.

vertices are born at the first time slice, and die at the same time. The diagrams for 0-critical cells are identical for the two experiments. For the case of 1-critical cells, we observe a similar distribution of life coordinates. Indeed, a high density of critical edges are born very early in the sequence and die around time slice  $t = 11$ . The main difference between the two experiments is that in the first one, there is an apparition of exactly one 2-critical cell, whereas in the second experiment we observe two of them being born. This can happen, as the extension algorithm is designed to produce close to the theoretical minimal number of critical cells, but it does not do so consistently.

**Stability Analysis.** We consider the robustness analysis described at the end of Section 8. More precisely, we plot the curves  $(\varepsilon, d_B(D_k, D_k^\varepsilon))_{\varepsilon \in E}$  for each dimension  $k \leq \dim(K)$ , where  $d_B$  is the Bottleneck distance. The corresponding plots are presented in Figure 17. Critical vertices seem not to be affected at all by the perturbation in the sampling process. Life coordinates of critical edges, on the other hand, are heavily affected. Finally, critical 2-cells seem to have life coordinates situated on the diagonal for any perturbation and thus produce almost consistently zero-Bottleneck distances.

## 9.2 The Triangle

In this subsection, we consider our simplicial complex  $K$  to be a triangle. We set  $G = K^{(0)}$ . If we choose an associated constant mapping

$$\mathbf{h} : \begin{cases} G \rightarrow \mathcal{C}^0(\mathbb{R}) \\ i \rightarrow h \end{cases},$$

where  $h(x) = \cos(2x)$  for all  $x \in \mathbb{R}$ , we end up with the parametric diagram shown in Figure 18. If instead we choose a non-injective function on the nodes, by taking  $h_1 = \cos(2\cdot)$ ,  $h_2 = \sin(3\cdot)$  and  $h_3 = \cos(x)$ , then we obtain the parametric diagram shown in Figure 19. For both experiments, we run the pipeline with no perturbation term, by considering a single time sequence. We choose the initial parameters so that we define

$$g_t : \begin{cases} G \rightarrow \mathbb{R} \\ i \rightarrow g_t(i) := h_i(5t) \end{cases},$$

where  $t \in \{0, \dots, 7\}$ . We have a sequence of 8 node labeling functions  $g_t : G \rightarrow \mathbb{R}$ .

**Interpretation.** The main observation behind this simple example is that injectivity of the initial node function heavily affects the output. More precisely, whether an input node function is injective or not drastically changes the way the extension algorithm runs and thus changes the way it produces critical cells. As a general behavior, we see that a non-injective node function is a better setting to produce a minimal number of critical cells.

**Stability Analysis.** Once again, we investigate the stability analysis described at the end of Section 8. We plot the curves  $(\varepsilon, d_B(D_k, D_k^\varepsilon))_{\varepsilon \in E}$  for each dimension  $k \leq \dim(K)$ , where  $d_B$  is the Bottleneck distance. The corresponding plots are presented in Figure 17. For the first experiment (injective setting), we obtain the diagram in Figure 20. The second experiment (non-injective setting) produces the diagram shown in Figure 21. In both cases, the procedure is deterministic and we obtain identity curves. In fact, the perturbation of the initial node function does not affect at all the output parametric diagram here.

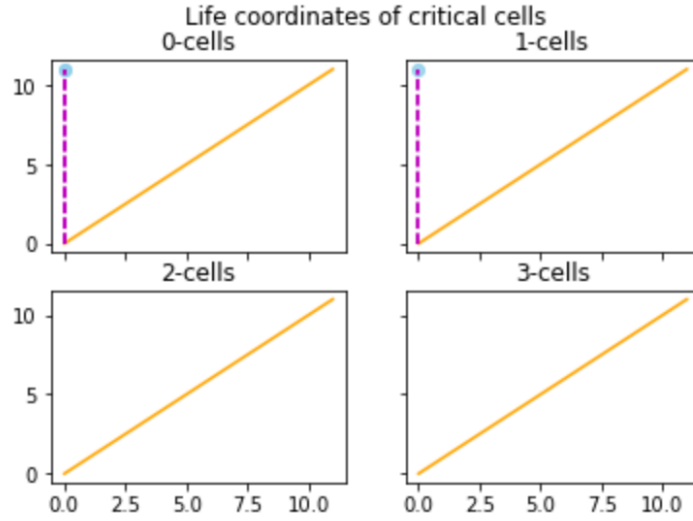


Figure 18: Parametric diagrams obtained with a tetrahedron as input and identical cosine waves on each vertex. Each parametric diagram corresponds to a specific dimension of critical cells, as indicated.

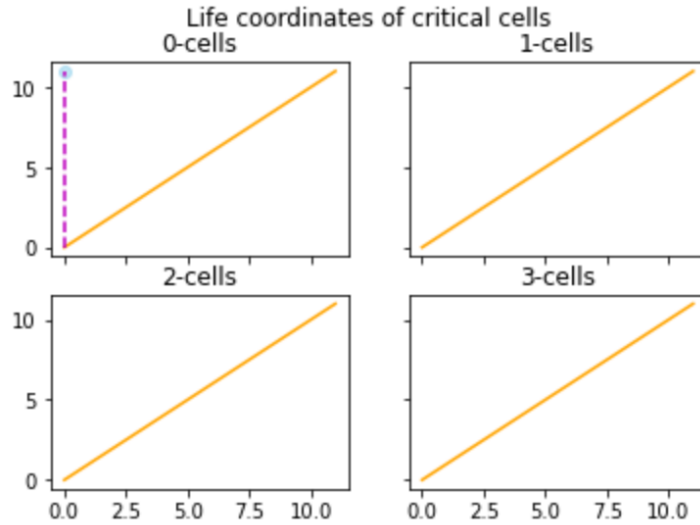


Figure 19: Parametric diagram obtained with a triangle as input and cosine and sine wave functions on each vertex. Each parametric diagram corresponds to a specific dimension of critical cells, as indicated.

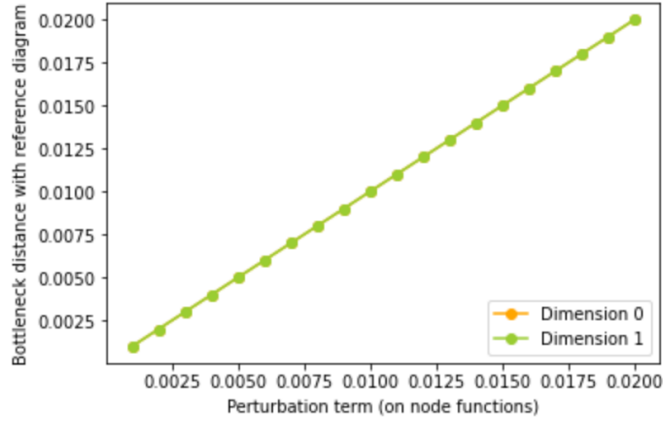


Figure 20: This figure represents the plotting of the curves  $(\varepsilon, d_B(D_k, D_k^\varepsilon))_{\varepsilon \in E}$  for the triangle with cosine waves on each vertex.

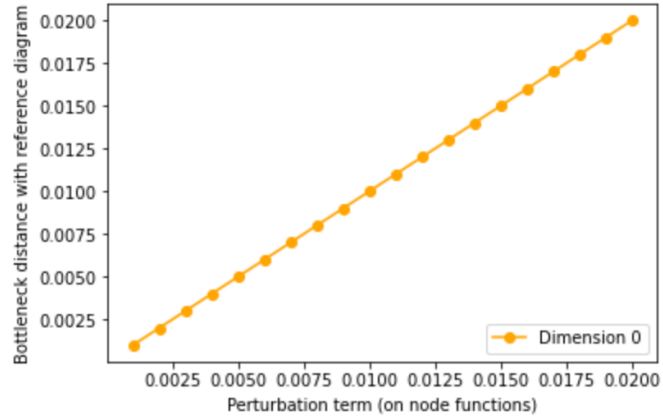


Figure 21: This figure represents the plotting of the curves  $(\varepsilon, d_B(D_k, D_k^\varepsilon))_{\varepsilon \in E}$  for the triangle with sine and cosine waves on each vertex.



### 9.3 The Stochastic Block Model

One of the graph classes that we use for the computations is the stochastic block model, having for main characteristic that it naturally forms a partitioning of its vertices into disjoint clusters, also called «communities».

**Definition 9.1.** *The stochastic block model  $\text{Block}(n, k, \{C_a\}_{a=1}^k, \{p_{a,b}\}_{a,b=1}^k)$  is a graph of  $n$  vertices built on  $k$  disjoint communities (or clusters), defined as follows. We consider all nodes, partitioned into  $k$  communities  $\{C_a\}_{a=1}^k$ , and draw an edge between  $i \in C_a$  and  $j \in C_b$  with probability  $p_{a,b}$ .*

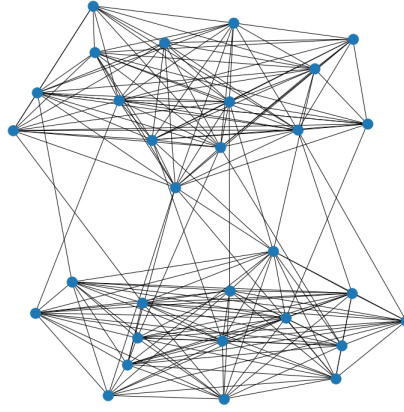


Figure 22: A stochastic block model generated on a total of  $n = 30$  nodes, for two clusters  $C_1$  and  $C_2$  with intra-cluster probabilities  $p_{1,1} = p_{2,2} = 0.7$  and inter-clusters probability  $p_{1,2} = 0.05$ . We set  $|C_1| = |C_2| = \frac{n}{2} = 15$ .

We run the pipeline on a stochastic block model  $G$  generated on a total of  $n = 24$  nodes, for four clusters  $C_1$  to  $C_4$  of cardinality  $\frac{n}{4} = 6$  with intra-cluster probabilities of 0.05 and inter-clusters probabilities of 0.8. The input graph is shown below, in Figure 23.

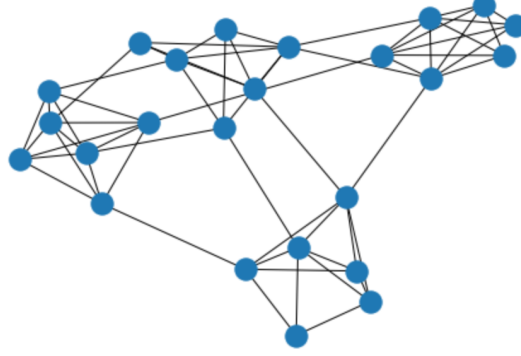


Figure 23: A stochastic block model generated on a total of  $n = 24$  nodes, for four clusters  $C_1$  to  $C_4$  with intra-cluster probabilities of 0.05 and inter-clusters probabilities of 0.8. We set  $|C_1| = |C_2| = |C_3| = |C_4| = \frac{n}{4} = 6$ .

The final output of the pipeline are the parametric diagrams (up to dimension  $k = 3$ ) of the critical cells obtained with the finite discrete Morse parametrization built from  $G$ . Once again, we consider sine and cosine waves as functions assigned to each node. We run two experiments and report the results. In the first experiment, we consider a sampling process such that in each cluster  $C_k$  has a similar mapping  $\mathbf{h} : C_k \rightarrow \mathbb{R}$  that is injective. In the second experiment, the sampling process is done in a way that each cluster  $C_k$  has a constant mapping, and this mapping is different for all clusters. Parametric diagrams for the first and second experiments are reported in figures 24 and 25. We observe a similar distribution of life coordinates between the two sets of diagrams. In this case, it thus seems the shape of the graph has more importance than the actual node values for the final output.

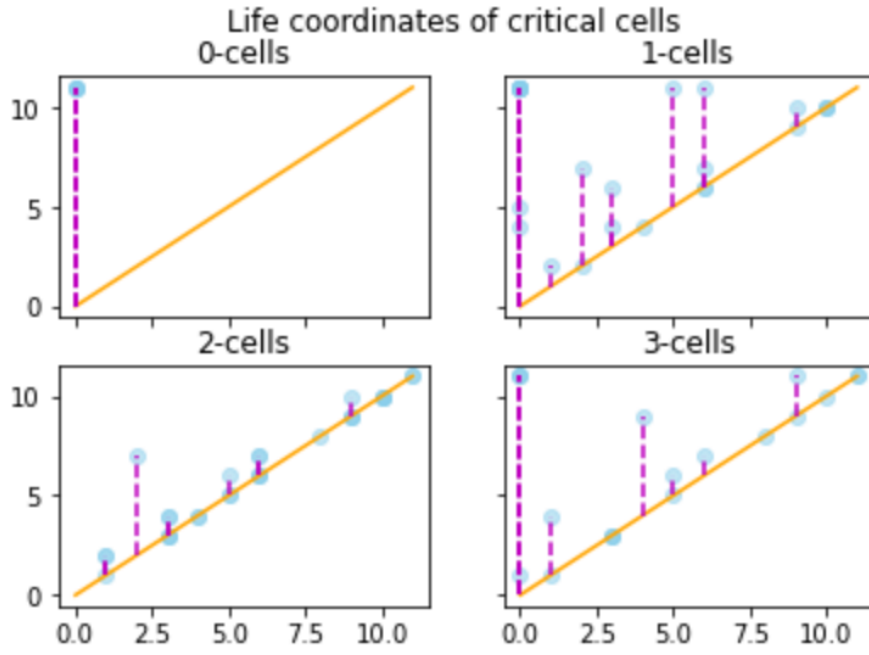


Figure 24: Parametric diagrams for the stochastic block model  $G$  with four clusters. Sampling process is the same for each cluster and injective within each single cluster.

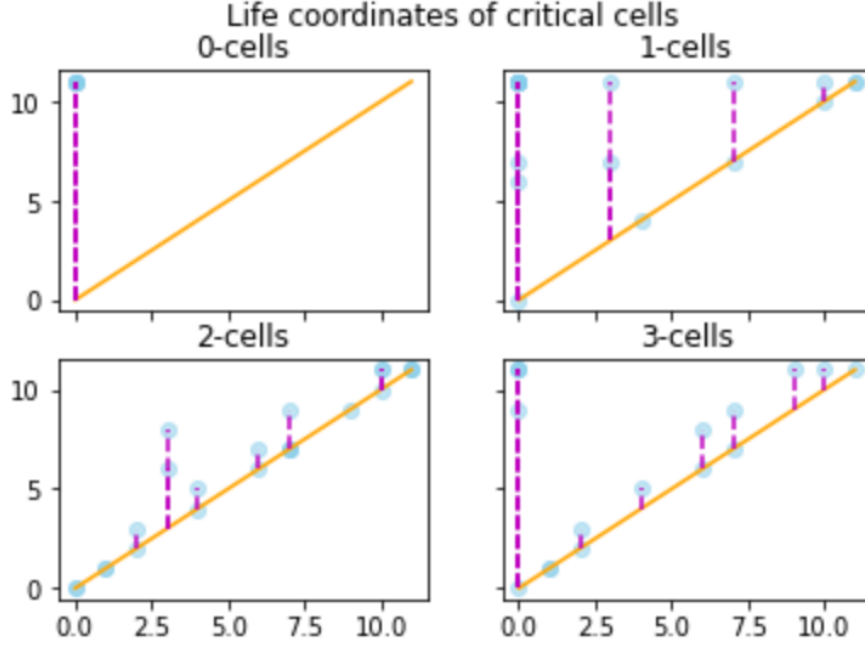


Figure 25: Parametric diagrams for the stochastic block model  $G$  with four clusters. Sampling process is different for each cluster. Each single cluster is assigned a constant mapping.

## 10 What next?

**Objective.** The content of this work aims, in particular, at developing ways to analyse the evolution of critical cells appearing along a sequence of real-valued vertex labelings  $\{g : K^{(0)} \rightarrow \mathbb{R}\}_{t=1}^n$  extended to discrete Morse functions  $\{f : K \rightarrow \mathbb{R}\}_{t=1}^n$  on a simplicial complex  $K$ . We know that, when attaining the minimum number of critical cells for a given pair  $(K, f_t)$  where  $f_t : K \rightarrow \mathbb{R}$  is a discrete Morse function, we have an elegant interpretation of what the term «critical» means. Indeed, we recall that 0-cells, 1-cells and maximum-dimensional cells of  $Y$  correspond to local minima, saddle points and local maxima respectively. Thus, parametric discrete Morse theory also provides tools to study the evolution (through time, perhaps) of fundamental geometric properties.

**Extension algorithms.** An interesting direction to take is the one of providing extension algorithms in higher dimensional labelings. More precisely, let  $0 \leq d \leq \dim(K)$ . One could provide a method to extend any real-valued labeling function  $g : K^{(d)} \rightarrow \mathbb{R}$  to a discrete Morse function  $f : K \rightarrow \mathbb{R}$ . For  $d = 2$ , this enables the application of discrete Morse theory-based analyses where the input data is a graph  $G$  that was assigned edge weights.

**Spectral theory-based node labelings.** An idea could be to consider initial node labelings according to a spectral theory principle, where a node  $i$  in time slice  $t$  would take the value of the  $i$ -component of the  $t$ -th eigenvector of the Laplacian of the graph given by  $K^{(0)}$ . The spectral theory setting might help understand the behavior of connected and almost disconnected components through time. If starting on a real-valued labeling sequence  $\{g : K^{(d)} \rightarrow \mathbb{R}\}_{t=1}^n$  for some  $1 \leq d \leq \dim(K)$ , and using an extension algorithm as mentioned above, then we may consider higher-order Laplacians defined for simplicial complexes. We refer to [SimplexLaplacians] for more details. This would enable the understanding of connected and almost connected components through the study of not only 0-critical cells but also higher-dimensional critical cells.

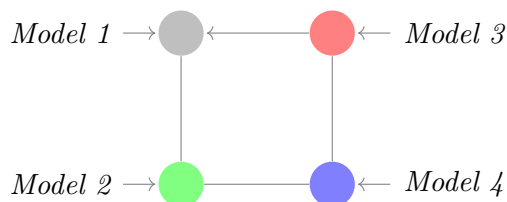
**Smooth Morse theory.** It seems like there still needs to be some work done in the context of understanding the links between the smooth and the discrete case. An interesting direction could be to translate the concept of *Cerf theory* in the discrete case. This would be related to the notions of birth and death as studied in this project.

**Birth-death diagrams.** In this project, we consider parametric diagrams rather than birth-death diagrams as we deal with Wasserstein and Bottleneck distances. However, birth-death diagrams encode more information than parametric diagrams do, and thus it would be interesting to define a notion of distance between birth-death diagrams.

**Biological Modeling of Neural Networks** We now give some perspective to our approach by considering the context of biological modeling of neural networks (for the purpose of studying neuron populations).

**Example 10.1** (Neuron Populations). *One could think of the input graph  $G$  as a neural network representing the generalized firing behavior of certain brain regions. More precisely, each node represents a specific neuron population (or a brain area) that share a biological feature, such as their firing*

model. By considering four of those populations, we are looking at the graph below, where **Model 1** could be, for example, the leaky integrate-and-fire model (LIF) and thus the function associated to the node of **Model 1** would be a LIF curve.



**Example 10.2** (The Stochastic Block Model for Neuron Firing Models). In the context of biological modeling of neural networks, one can extend the previous example by replacing every node (i.e. every neuron population) by a cluster of neurons. To this end, one can take as input graph  $G$  a stochastic block model where nodes within the same community share similar firing models.

## References

- [1] Henry King, Neza Mramor, Kevin Knudson. *Birth and Death in Discrete Morse Theory*, 2016.
- [2] Henry King, Neza Mramor, Kevin Knudson. *Generating Discrete Morse Functions from Point Data*, 2005.
- [3] Robin Forman. *A User's Guide to Discrete Morse Theory*, 2002.
- [4] Harish Kannan, Emil Saucan, Indrava Roy, Areejit Samal. *Persistent homology of unweighted complex networks via discrete Morse theory*, 2019.
- [5] Abubakr Muhammad, Magnus Egerstedt. *Control Using Higher Order Laplacians in Network Topologies*.